Theoretical Chemistry Accounts (2025) 144:1
https://doi.org/10.1007/s00214-024-03154-5

RESEARCH

Theoretical prediction of the dehydration mechanism of 1, 3-butanediol as a potential biofuel surrogate

Mohamed A. Abdel-Rahman[1,2] · Mohammed K. Morse[2] · Hao Zhao[1]

Received: 5 July 2024 / Accepted: 19 October 2024 / Published online: 2 December 2024

Abstract

The current study represents a comprehensive theoretical attempt to elucidate the dehydration mechanism of 1,3-Butanediol (1,3-BDO) using density functional methods, M06-2X and ωB97XD, as well as the ab initio composite method, complete basis set-quadratic Becke3 (CBS-QB3). The study revealed the atomization enthalpy (AE), bond dissociation energy (BDE), ionization energies (IE), and electron affinities (EA) of the parent molecule 1,3-BDO and all formed products at different levels of quantum chemistry. The obtained results were also compared against available theoretical and experimental data for mechanism validation. Thermodynamically, the results illustrated that despite the low barrier height of TS2, the pathway leading to 1,3-butadiene (1,3-BD) formation is considered the most favorable, while the formation of 1,2-butadiene (1,2-BD) is less likely. From the analysis of BDE, the inner alcoholic OH group is stronger than the terminal one by 6.4 kJ/mol, and the terminal alcoholic O–H bond is weaker by 6.8 kJ/mol, indicating the higher acidity of the terminal alcoholic OH group.

Keywords DFT; Ab initio; 1 · 3-butanediol; Thermochemistry

1 Introduction

The search for sustainable green energy resources has become a global priority due to the serious risks posed by fossil fuels to human health and their contribution to global warming. Among various renewable energy sources, biofuel is considered a promising alternative to fossil fuels, offering the potential to significantly reduce greenhouse gas emissions and mitigate the adverse effects of climate change [1–4]. Multi-functional biofuel molecules have several advantages over unifunctional biofuels, as their multiple functional groups can enhance the ignition and combustion properties of these fuels compared to unifunctional ones [5–8].

1,3-Butanediol (1,3-BDO) is a non-natural, optically active diol compound that exists as a colorless, odorless liquid and is soluble in water and ethanol [9]. It is a valuable chemical used as a key intermediate in the synthesis of pharmaceuticals and various industrial compounds, such as pheromones, fragrances, and insecticides [10]. The production of 1,3-BDO can be achieved through the self-condensation of acetaldehyde in an alkaline medium. This reaction produces 3-hydroxybutanal (acetaldol) as an intermediate, which subsequently forms 1,3-BDO through dehydrogenation [11].

Recently, significant efforts have been made to produce 1,3-BDO from various biomass sources [12, 13]. Kataoka et al. [12] conducted a study on the production of 1,3-BDO from glucose using Escherichia coli MG1655 lacIq. The authors achieved a yield of 1,3-BDO up to 9.05 g/L (100.4 mM) with 98.5 ± 0.2% enantiomeric excess of (R)-1,3-BDO, which is considered the highest yield of 1,3-BDO produced from glucose. Liu et al. [13] explored the production of 1,3-BDO from biomass through the hydrogenolysis of 1,4-anhydroerythritol over a Pt–WOx/SiO2 catalyst, achieving a yield of up to 54%.

Experimental and theoretical combustion chemistry of unifunctional biofuels such as n-butanol and 2-butanol has gained sufficient attention in recent years [14–24]. However, studies on bifunctional molecules remain relatively rare [5–8, 25–27].

✉ Mohamed A. Abdel-Rahman
Mohamedadel@pku.edu.cn

✉ Mohammed K. Morse
Mohammed.KhMoM@sci.suezuni.edu.eg

[1] College of Engineering, Peking University, Beijing 100871, China

[2] Department of Chemistry, Faculty of Science, Suez University, Suez 43518, Egypt

Experimentally, the dehydration of 1,3-BDO and its isomers was studied by Ward et al. [28] using Brønsted acids and heterogeneous systems, including γ-alumina or the zeolite ZSM-5. Sun et al. [29] discussed the dehydration mechanism of C4 unsaturated alcohols such as 3-buten-1ol, 2-buten-1-ol and 3-buten-2-ol to produce 1,3-butadiene (1,3-BD) over various solid catalysts such as Al_2O_3, SiO_2-Al_2O_3, and TiO_2, as well as metal oxides like Yb_2O_3 and CeO_2. Kurniawan et al. [30] studied the gas phase dehydration of 1, 3-BDO to 1, 3-BD over WO_3/SiO_2 catalyst. The authors used various silica-supported metal oxides ($MxOy/SiO_2$). With the WO_3/SiO_2 catalyst showing the highest activity for BD production.

Based on the structure of 1,3-BDO and insights from similar studies [5–8, 25–27], we expect that the pyrolysis of 1,3-BDO could yield better results compared to unifunctional biofuels such as n-butanol and 2-butanol, owing to its higher energy content and oxygen ratio. In this work, we aim to shed some light on the different pathways of water elimination reactions from 1,3-BDO, in hopes of drawing attention to this molecule for further theoretical and experimental investigation.

2 Computational details

2.1 Quantum and thermodynamics calculations

All computational calculations were performed using Gaussian 09 [31] and 16 packages [32], while molecular visualization was carried out using Chemcraft software [33]. The geometrical optimizations of reactants (R), transition states (TS), and products (P) were conducted using a combination of density functional theory: the Minnesota M06-2X hybrid meta-functional with 54% HF exchange [34], and the long range non –covalent interaction functional ωB97XD [35], both with the correlated consistent polarized valence triple-zeta basis set (cc-pvTZ). Since the energies from M06-2X and B97XD energies are not sufficiently precise, the electronic energies were further refined using the ab initio complete basis set-quadratic Becke3 (CBS-QB3) method, developed by Petersson et al. [36–38]. The composite CBS-QB3 method includes geometry optimization and frequency calculation at the B3LYP/6-311G(d, p) level followed by CCSD(T)/6–31 + G (d), MP4SDQ/6–31 + G (d,p), and MP2/6–311 + G (2df,2p) single point energy calculations with CBS extrapolation.

For further reliability, we used the G4 [38, 39] to assess the accuracy of the methods employed. The transition states for all possible H_2O elimination reactions were located using the eigenvector-following (EF) optimization technique implemented in the Gaussian suite of programs. Vibrational frequency calculations were conducted at the same level of theory to characterize the nature of those points as minima (real frequencies) or transition state (only one imaginary frequency) and to correct energies for zero-point (ZPE) and thermal contributions at 298 K. The connections between different transition states (TSs) with their relative reactants and products were computed using the intrinsic reaction coordinates (IRC) at M06-2X/cc-pvTZ level [40, 41]. The IRC calculations were performed with a step size 0.1 $amu^{1/2}$ Bohr, with 15 steps in both forward and backward directions.

2.2 Thermodynamical calculations

The gas-phase enthalpies of formation for 1, 3-BDO and all released products were calculated at standard conditions of temperature and pressure (STP) using the atomization energy approach (Eq. (1)):

$$\Delta H_f^0(M) = E_e(M) + ZPE(M) + \left[H_{298}(M) - H_0(M)\right] - \sum_i^{atoms} \left[E_e(X_i) + \left[H_{298}(X_i) - H_0(X_i)\right]\right] + \sum_i^{atoms} \Delta H_{f,gas}^0(X_i) \quad (1)$$

where $E_e(M)$, and$E_e\left(X_i\right)$ are the calculated electronic energies of molecule M and the electronic energy of the ith atom X, respectively. $[H_{298}(M)–H_0(M)]$ and $[H_{298}(X_i)–H_0(X_i)]$ are the thermal corrections to the enthalpy for the molecule M and the individual atoms X, respectively.

Ionization energy (IE) and electron affinity (EA) are crucial for calculating various molecular properties such as softness, hardness, electronegativity, and electrophilicity [42, 43].

IE is the minimum amount of energy required to remove an electron from a neutral molecule, resulting in the formation of a positive cation (Eq. (2)). Conversely, EA is the energy released when a neutral molecule gains a new electron (Eq. (3))

$$IE = E\left(N^+\right) - E(N) \quad (2)$$

$$EA = E(N) - E(N^-) \quad (3)$$

where $E(N^+)$ is the computed energy of the cation, E(N) is the energy of neutral molecule, and $E(N^-)$ is the computed energy of the anion, all evaluated at the same level of computation.

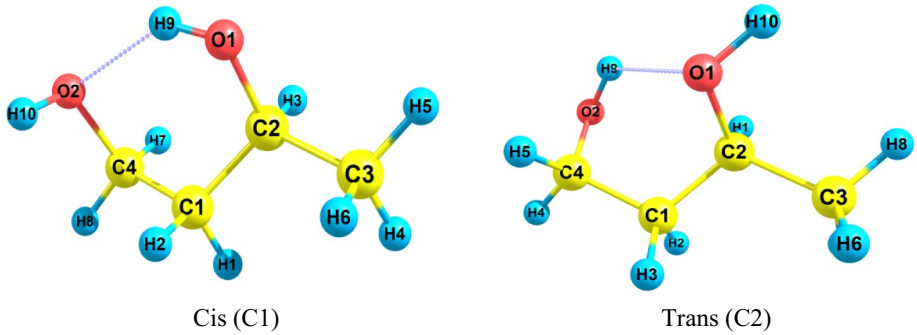

Fig. 1 Different conformers of 1,3-butanediol

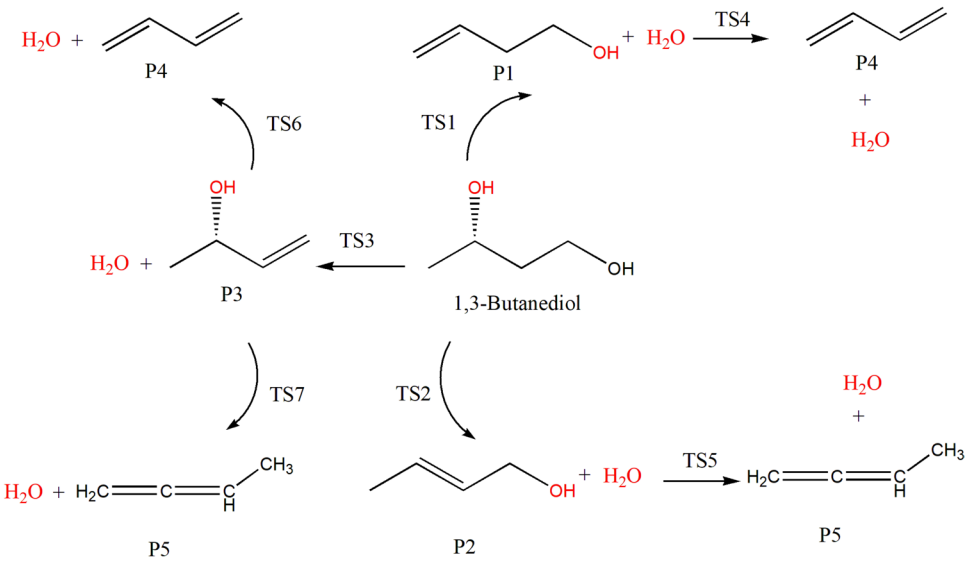

Fig. 2 Different possible water elimination reactions from 1, 3-Butanediol

3 Results and discussion

3.1 Energetics and thermodynamic parameters

3.1.1 Conformers stability & dehydration mechanism

1, 3-BDO molecule has two stable conformers: Cis (C1) and Trans (C2), as shown in Fig. 1. The C1 form is more stable than the C2 form by 5 and 6 kJ/mol at M06-2X/cc-pvTZ and CBS-QB3 levels, respectively (Fig.S1). Therefore, the current study will base on the most stable conformer, C1, at CBS-QB3 method. Figure 2 illustrates various possible pathways for the dehydration mechanisms of 1, 3-BDO. From Fig. 2, it is evident that the terminal OH group can initiate the reaction through TS3 to form but-3-en-2-ol (P3) as an intermediate enol compound, which can then decompose via TS6 and TS7 to produce the diene molecules, 1,3-butadiene (1,3-BD, P4) and 1,2-butadiene (1,2-BD, P5), respectively. The inner OH group can initiate the reaction through TS1 and TS2.

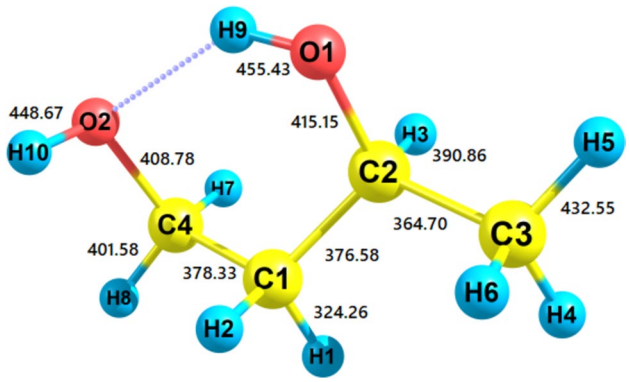

Fig. 3 Bond dissociation energy (BDEs, kJ/mol) of 1, 3-BDO at CBS-QB3

TS1 leads to the intermediate but-3-en-1-ol (P1), which decomposes via TS4 to produce 1, 3-BD (P4). The TS2 results in the intermediate but-2-en-1-ol (P2), which ultimately produces 1, 2-BD (P5) as the final product.

3.1.2 Bond dissociation energies (BDEs)

Bond dissociation energies (BDEs) are crucial for evaluating the strength of different bonds. Figure 3 shows the BDEs of 1,3-BDO calculated using the CBS-QB3 method. Among all the C-H bonds in 1,3-BDO, the C1-H1 bond is the weakest σ-bond at 324 kJ/mol, which can be attributed to its high acidity. This is followed by the C2-C3 bond, with a BDE of 365 kJ/mol. In contrast, the O1-H9 bond is the strongest, with a BDE of 455 kJ/mol. These values suggest that the C1-H1 and C2-C3 bonds will likely be the dominant pathways for simple bond fission at high temperatures.

The C1-C2 and C1-C4 bonds exhibit comparable energies, with BDEs of 377 kJ/mol and 378 kJ/mol, respectively. The terminal O2-H10 bond (449 kJ/mol) and the C4-O2 bond (409 kJ/mol) are weaker than the inner O1-H9 bond (455 kJ/mol) and the C2-O1 bond (415 kJ/mol) by 6.8 kJ/mol and 6.4 kJ/mol, respectively. This indicates that the terminal OH group is more likely to initiate dehydration reactions. It is also noteworthy that the calculated BDEs for the terminal O2-H10, C4-O2, inner O1-H9, and C2-O1 bonds are very similar to those observed in 2-butanol, n-butanol [7, 17], and 2-methoxyethanol [6, 7].

3.1.3 Enthalpies of formation, ionization energies, and *electron* affinities

Tables 1 and 2 summarize the computed ionization energies (IE), electron affinities (EA), and enthalpies of formation ΔH_f^{298} using the CBS-QB3 method, compared to available experimental results and the Argonne Active Thermochemical Tables (ATcT). The correlation between experimental and theoretical CBS-QB3 results for AE and IE of 1,3-BDO and all released products is shown in Fig. 4. The obtained results of IE and EA provide insight into the stability of different molecules. Molecules with high IE and EA values tend to be more stable than those with lower values. Additionally, molecules with lower enthalpies of formation are more likely to form during the course of a reaction.

From Table 1, 1-buten-3-ol ($CH_2=CHCH(OH)CH_3$) has the highest IE at 9.77 eV and EA of -1.09 eV, followed by 1-buten-4-ol ($CH_2(OH)CH_2CH=CH_2$) with an IE of 9.39 eV and an EA of -1.13 eV. The calculated values for 1, 3-BD (P4) are slightly higher than those obtained for 1, 2-BD (P5). This difference can be attributed to π-electron conjugation.

From Table 2, the computed enthalpy of formation ΔH_f^{298} shows that the parent compound 1, 3-BDO, has -456.90 kJ/mol, which is slightly lower than the experimental value of -447.10 [60]. The computed enthalpies of formation using the CBS-QB3 method show good

Table 1 Ionization Energy (IE, eV) and electron affinity (EA, eV) for 1,3-DBO and all released products during the dehydration mechanism at CBS-QB3

Species	IE	IE/Exp	EA	EA/Exp
$CH_2(OH)CH_2CH(OH)CH_3$	9.51	–	−0.64	0.008 ± 0.001 [a]
$CH_2(OH)CH_2CH=CH_2$	9.39	9.56 ± 0.05[b]	−1.13	–
$CH_2(OH)CH=CHCH_3$	9.07	9.13[c]	−1.70	–
$CH_2=CHCH(OH)CH_3$	9.77	9.53[c]	−1.09	–
$CH_2=CHCH=CH_2$	8.99	9.082 ± 0.004[d]	−0.68	–
$CH_2=C=CHCH3$	9.17	9.33 ± 0.02[e]	−1.01	–
H_2O	12.54	12.65 ± 0.05[f]	−0.86	–
$CH_3C(OH)(CH_3)CH_2CH_3$	9.42	9.80[g]	−0.54	–
$CH_3CH(OH)CH_2CH_3$	9.87	9.88 ± 0.03[h]	−0.72	–
$CH_2(OH)CH_2CH_2CH_3$	10.23	10.10 ± 0.05[i]	−0.54	–
C_2H_6	11.56	11.52[j]	−0.82	–
C_2H_5OH	10.45	10.46 ± 0.02[k]	−0.75	–
CH_4	12.63	12.61 ± 0.01[L]	−0.84	–
CH_3OH	10.83	10.84 ± 0.07[m]	−0.76	–
$CH_3C(CH_3)_2CH_2(OH)$	9.38	9.72 ± 0.05[n]	−0.57	–
$CH_3CH(OH)CH_2CH_2CH_3$	9.54	9.78 ± 0.07[m]	−0.59	–
CH_3 $CH_2CH(OH)CH_2CH_3$	9.53	9.78 ± 0.07[m]	−0.69	–
$CH_2(OH)CH_2CH_2CH_2CH_3$	10.30	10.38 [o]	−0.68	–
$CH_3CH(OH)CH_3$	9.99	10.15 ± 0.07[m]	−0.70	–
C_3H_8	10.95	10.94 ± 0.05[p]	−0.73	–
$CH_2(OH)CH_2CH_3$	10.32	10.32 ± 0.02[k]	−0.57	–

[a] Ref. [44], [b] Ref. [45], [c] Ref. [46], [d] Ref. [47], [e] Ref. [48], [f] Ref. [49], [g] Ref. [50], [h] Ref. [51], [i] Ref. [52], [j] Ref. [53], [k] Ref. [54], [L] Ref. [55], [m] Ref. [56], [n] Ref. [57], [o] Ref. [58], [p] Ref. [59]

Table 2 Enthalpy of formation using atomization energy approach (kJ/mol) for all released species at CBS-QB3

Species	$\Delta H^0_{f,298}$(kJ/mol)		
	AE	Exp	Argonne Active Thermochemical Tables (ATcT) [i]
$CH_2(OH)CH_2CH(OH)CH_3$	−456.90	−447.10[a]	–
$CH_2(OH)CH_2CH=CH_2$	−146.00	–	–
$CH_2(OH)CH=CHCH_3$	−155.39	–	–
$CH_2=CHCH(OH)CH_3$	−161.92	–	–
$CH_2=CHCH=CH_2$	118.23	108.80 ± 0.79 [b]	111.17 ± 0.29
$CH_2=C=CHCH3$	168.11	165.40 ± 1.20 [c]	162.56 ± 0.42
H_2O	−243.65	−241.83 [d]	−241.81 ± 0.02
CH_4	−74.55	−74.60 ± 0.30 [e]	−74.51 ± 0.04
CH_3OH	−204.63	−205. 00 ± 10.00 [f]	−200.84 ± 0.14
C_2H_6	−82.75	−84.00 ± 0.40 [e]	−84.01 ± 0.12
C_2H_5OH	−237.18	−234.00 ± 2.00 [f]	−234.89 ± 0.19
C_3H_8	−102.19	−104.70 ± 0.50 [g]	−104.99 ± 0.15

[a] Ref. [61], [b] Ref. [62], [c] Ref. [63], [d] Ref. [64], [e] Ref. [65], [f] Ref. [66], [g] Ref. [67], [i] Ref [68–72]

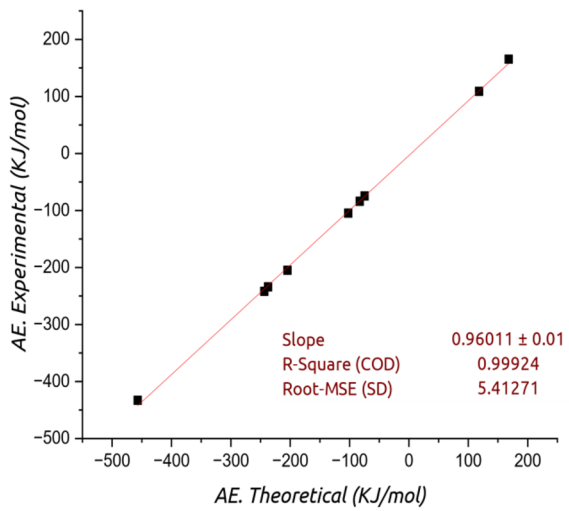

a) Correlation between experimental and theoretical results of enthalpy of formation from AE approach.

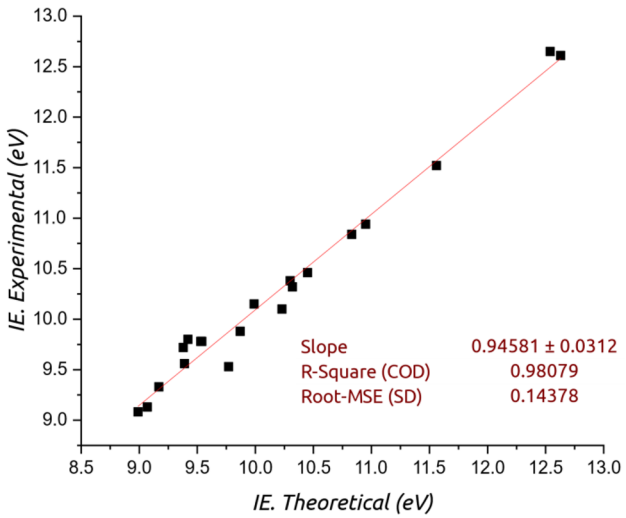

b) Correlation between experimental and theoretical (adiabatic) IE.

Fig. 4 Correlation between experimental and theoretical results (at the CBS-QB3 method) of enthalpy of formation from AE approach (Fig. 4a) and IE (Fig. 4b)

agreement with available experimental data and the values from the Argonne Active Thermochemical Tables (ATcT), providing confidence in our theoretical calculations.

Among the compounds, 1-buten-3-ol ($CH_2=CHCH(OH)CH_3$) has the lowest enthalpy of formation at -161.92 kJ/mol, followed by 2-buten-4-ol ($CH_2(OH)CH=CHCH_3$) at -155.39 kJ/mol, and 1-buten-4-ol ($CH_2(OH)CH_2CH=CH_2$) at -146.00 kJ/mol. The final products 1, 3-BD (P4) and 1, 2-BD (P5) have enthalpies of formation of 118.23 kJ/mol and 168.11 kJ/mol, respectively.

The Mean Signed Error (MSE), Mean Absolute Error (MAE), and Root Mean Square Error (RMSE) were calculated to verify the validity of the theoretical results from the CBS-QB3 method against the experimental results for AE, IE, and EA values. MSE, MAE, and RMSE were estimated using Eqs. (4–6), respectively.

$$MSE = \frac{\sum \left(\theta_t - E_t\right)}{n} \tag{4}$$

$$MAE = \frac{\sum |\theta_t - E_t|}{n} \quad (5)$$

$$RMSE = \sqrt{\frac{\sum (\theta_t - E_t)^2}{n}} \quad (6)$$

where θ_t is theoretical (CBS-QB3) value, E_t is the experimental value, and n is the total number of observations. The MSE, MAE, and RMSE values for IE were 0.125, -0.081, and 0.168 eV, respectively. Similarly, for AE, the corresponding values were 3.935, 0.308, and 5.93 eV, respectively. These results, along with the correlation between CBS-QB3 results and experimental values (shown in Fig. 4) demonstrate strong harmony between the computational results using the CBS-QB3 method and available experimental results. The data from Fig. 4 can also be used to predict to the expected experimental value for unknown species based on their CBS-QB3 results.

3.2 Structures and energies

From Fig. 2, the dehydration mechanism of 1,3-BDO proceedS through seven transition states (TS1-TS7). Dehydration of 1,3-BDO is a two-step reaction mechanism. The first step involves passing through transition states TS1, TS2, and TS3 to produce the intermediates P1, P2, and P3, respectively. In the second step, the intermediates P1, P2, and P3 undergo further transformations via TS4, TS5, and TS6 to form the final products P4 and P5.

The optimized structures of 1,3-BDO and all transition states (TS1–TS7) are depicted in Fig. 5, while Fig. 6 and Table 3 present the energy profile diagram and thermodynamic parameters for the dehydration of 1,3-BDO calculated using CBS-QB3, M06-2X, and ωB97XD methods. The accuracy of CBS-QB3 was examined against the high-level ab initio G4 method and good agreement was observed, with differences of less than 6 kJ/mol.

In the first step of the reaction, TS1 involves the elimination of H_2O through the reaction of the hydroxyl (O1H9) group attached to C2 atom and one of hydrogen atom from the terminal methyl group (C3 atom). Inspection of TS1 reveals that the formed H5–O1 and C3–C2 bonds are shortened by 1.34 Å (52.04%) and 0.093 Å (6.11%), respectively. In contrast, the broken $C2-O1$ and $C3-H5$ bonds are elongated by 0.42 Å (29.59%) and 0.35 Å (32.42%), respectively. The reaction results in the formation of intermediate P1 with a barrier height and reaction energy 281 and 16 kJ/mol, respectively at CBS-QB3.

TS2 proceeds via the transfer of a H atom from one of the internal CH_2 groups (C1 atom) to the hydroxyl (O1H9) group linked to the C2 atom. Investigation of TS2 indicates that the broken C2-O1 and C1-H2 bonds are elongated by 0.72 Å (50.21%) and 0.16 Å (12.86%), respectively, while the formed O1-H2 and C1-C2 bonds are shortened by 1.27 Å (47.50%) and 0.12 Å (8.01%), respectively. This reaction results in the formation of intermediate P2, which has the lowest barrier height in the potential energy profile at 278 kJ/mol, and the reaction energy is exothermic by 8 kJ/mol.

TS3 is formed by the migration of a H atom from the internal methyl CH_2 group (C1 atom) to the terminal hydroxyl (O2-H10) group. The reaction proceeds with the highest barrier height of 285 kJ/mol and the lowest reaction energy of 3 kJ/mol, making it the least endothermic reaction among all dehydration reactions of 1, 3-BDO. During the progress of this reaction, the formed C1-C4 and O2-H2 bonds are shortened by 0.12 Å (7.85%) and 1.42 Å (51.56%), respectively, while the broken C1-H2 and O2-C4 bonds are elongated by 0.22 Å (20.40%) and 0.58 Å (40.40%), respectively.

In the second step of the reaction, the final product P4 is formed by the conversion of intermediates P1 and P3 via transition states TS4 and TS6, respectively. The conversion of P1 to P4 occurs with a low barrier height of 265 kJ/mol and reaction energy of 22 kJ/mol, while the conversion of P3 to P4 requires a higher barrier height of 271 kJ/mol and reaction energy of 9 kJ/mol, relative to the energy of P1.

In TS4, the broken C4-O1 and C1-H2 bonds are elongated by 0.36 Å (25.51%) and 0.38 Å (34.37%), respectively, while the formed C1-C4 and H2-O1 bonds are shortened by 0.09 Å (6.02%) and 1.37 Å (52.63%), respectively. In TS6, the formed C2-C3 and H4-O1 bonds are decreased by 0.11 Å (6.96%) and 1.35 Å (50.56%), respectively, while the broken C2-O1 and C3-H4 bonds are elongated by 0.57 Å (39.75%) and 0.25 Å (23.26%), respectively.

The final product P5 is formed by the transformation of the two intermediates P2 and P3 via transition states TS5 and TS7, respectively. During the progress of TS5, the formed C1-C4 and H1-O1 bonds are shortened by 0.09 Å (5.64%) and 2.27 Å (66.23%), respectively, while the broken C4-O1 and C1-H1 bonds are elongated by 0.38 Å (26.83%) and 0.45 Å (41.10%), respectively. The reaction proceeds with a barrier height and reaction energy of 324 kJ/mol and 33 kJ/mol, respectively, while the conversion of P3 to P5 via TS7 requires barrier heights and reaction energies of 320 kJ/mol and 38 kJ/mol, respectively. In TS7, the formed C1-C2 and O1-H1 bonds are shortened by 0.09 Å (5.69%) and 2.25 Å (65.74%), respectively, while the broken C2-O1 and C1-H1 bonds are elongated by 0.44 Å (30.69%) and 0.41 Å (37.87%), respectively.

According to Hammond's postulate, in endothermic reactions, the transition states are closer to the products than to the reactants [73]. From Fig. 6 and Table 3, it is evident that the formation of intermediate P3 is the most favorable among all first- step reaction intermediates, with a reaction enthalpy $\Delta H_{298} = 51$ kJ/mol and a reaction energy of

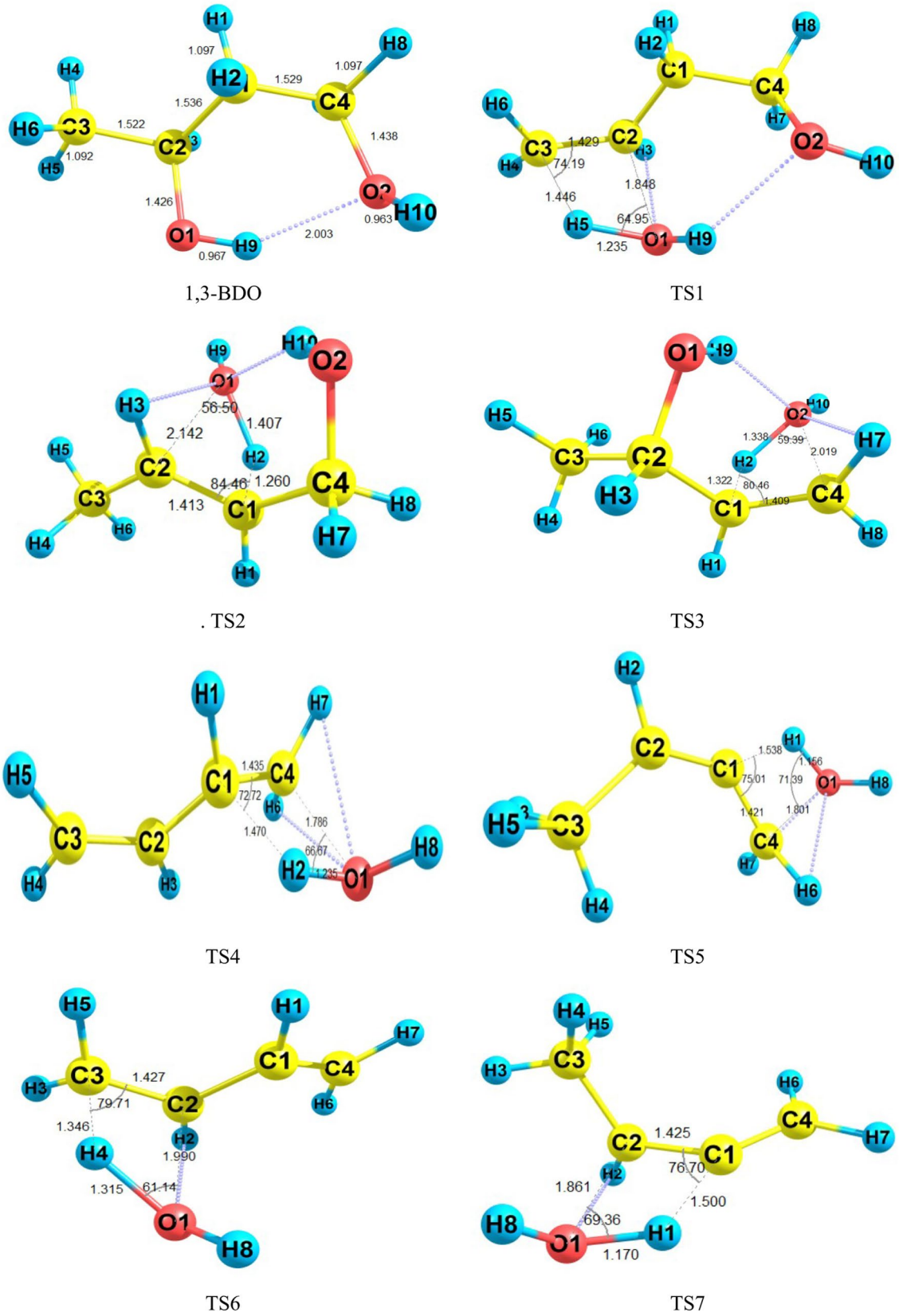

Fig. 5 Optimized structures of 1, 3-BDO and all transition states (bond lengths in Å and angles in degrees) at the B3LYP/6-311G (d, p) level (the optimization level at the CBS-QB3 composite method)

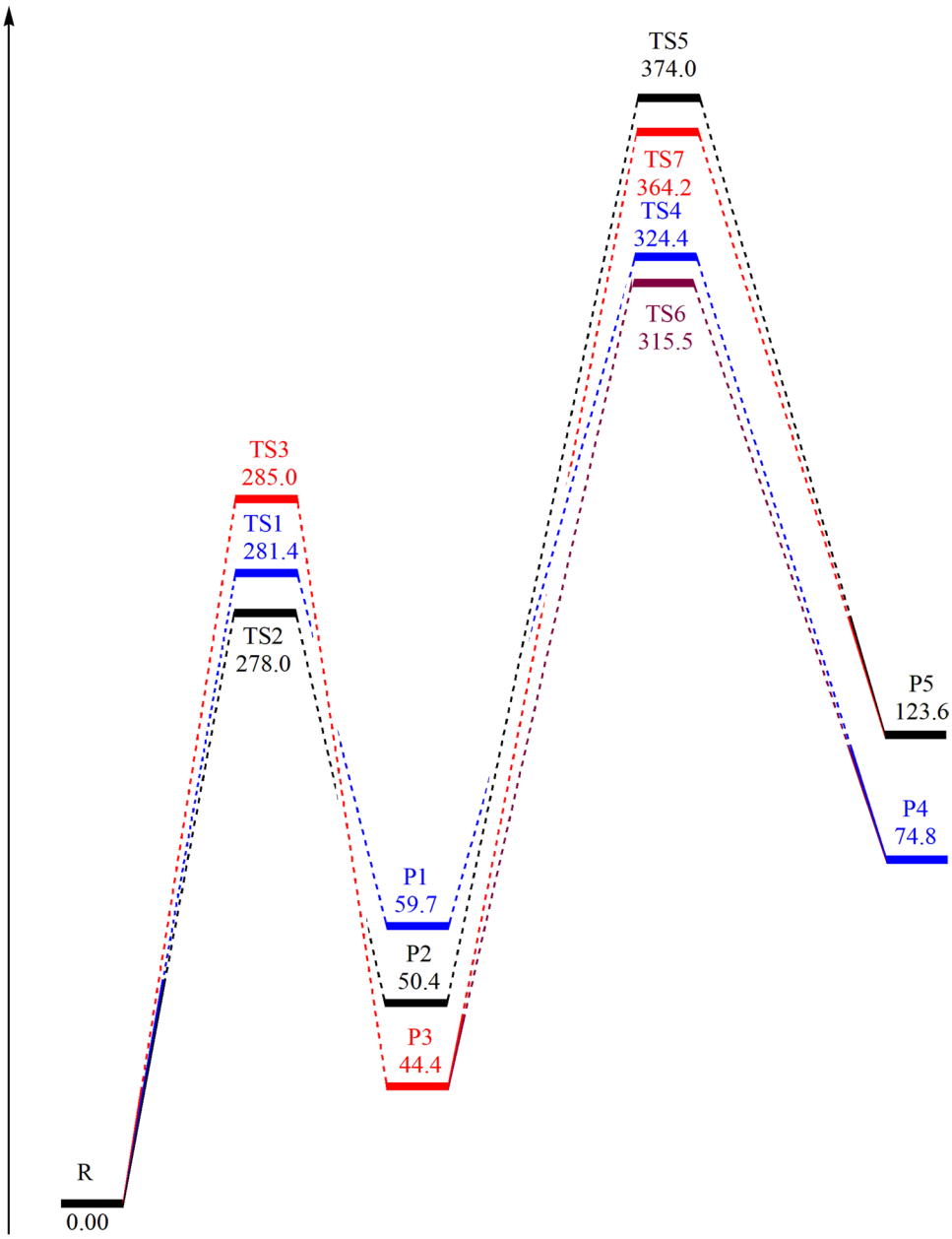

Fig. 6 Energy profile (ΔE_{0K}) in kJ/mol for the transition states and products of the dehydration of 1,3-BDO calculated using the CBS-QB3 method

$\Delta G_{298} = 3$ kJ/mol. However, it requires a very high transition state energy TS3 ($\Delta E^{\pm}_{0} = 285$ kJ/mol) compared to the most stable transition state, TS2 ($\Delta E^{\pm}_{0} = 278$ kJ/mol) and TS1 ($\Delta E^{\pm}_{0} = 281$ kJ/mol).

The formation of P4 through TS6 is the most favored thermodynamically and kinetically during the dehydration mechanism, with $\Delta H_{298} = 88$ kJ/mol and $\Delta G_{298} =$—7 kJ/mol. This is lower than the energies required for P5 ($\Delta H_{298} = 138$ kJ/mol, $\Delta G_{298} = 41$ kJ/mol), indicating the higher stability of P4 over P5.

By comparing the barrier heights of TS4 and TS6, we observe that TS6 has a lower barrier ($\Delta E^{\pm}_{0} = 316$ kJ/mol) than TS4 ($\Delta E^{\pm}_{0} = 324$ kJ/mol) by 8.85 kJ/mol. This suggests that the formation of P4 occurs through TS3 and TS6, passing through the formation of P3, while facing significant competition from the reaction that passes through TS1 and TS4.

Figure 7 illustrates the correlation between barrier heights (kJ/mol) at the CBS-QB3 method compared to those obtained at M06-2X/cc-pvTZ level (Fig. 7a) and at the ωB97XD /cc-pvTZ level (Fig. 7b). The results demonstrate good agreement between CBS-QB3 and M06-2X/cc-pvTZ results compared to those obtained at the ωB97XD / cc-pvTZ level.

Intrinsic reaction coordinates (IRC) were calculated at the M06-2X/cc-pvTZ level because the M06-2X hybrid

Table 3 Relative reaction energies (kJ/mol) at CBS-QB3, G4 (in bold), M06-2X/cc-pvTZ (in *italic*), and ωB97XD/cc-pvTZ (in parentheses)

Species	CBS-QB3				DFT/cc-pvTZ			
	Imaginary frequency(cm^{-1})	$\Delta E_o^{\ddagger}$	$\Delta H_{298}^{\ddagger}$	$\Delta G_{298}^{\ddagger}$	Imaginary frequency(cm^{-1})	$\Delta E_o^{\ddagger}$	$\Delta H_{298}^{\ddagger}$	$\Delta G_{298}^{\ddagger}$
R		0.00	0.00	0.00		0.00	0.00	0.00
TS1	− 1984.74	281.42 277.25	281.66	281.34	*− 1818.76 (− 1945.32)*	*275.55* (271.637)	*275.38* (271.24)	*276.03* (272.58)
TS2	− 1364.14	277.97 274.25	278.81	277.11	*− 1812.46 (− 1502.73)*	*279.03* (273.18)	*280.17* (274.23)	*277.95* (272.12)
TS3	− 1721.27	284.98	286	283.59	*− 1918.55 (− 2018.62)*	*281.84* (280.65)	*282.65* (281.57)	*280.42* (279.19)
TS4	− 1950.64	324.38 318.00	331.46	282.23	*− 1822.15 (− 1972.98)*	*331.15* (330.95)	*337.81* (337.63)	*289.57* (289.42)
TS5	− 1713.77	373.97 368.50	382.12	330.11	*− 1198.62 (− 1550.46)*	*383.28* (381.58)	*391.38* (389.5)	*337.92* (337.7)
TS6	− 1957.92	315.53	323.41	272.88	*− 1979.27 (− 2020.50)*	*328.51* (323.82)	*335.48* (330.94)	*287.05* (282.3)
TS7	− 1758.08	364.19	372.17	321.44	*− 1059.12 (− 1513.93)*	*374.55* (370.96)	*381.73* (378.5)	*332.85* (328.77)
		ΔE_o	ΔH_{298}	ΔG_{298}		ΔE_o	ΔH_{298}	ΔG_{298}
P1		59.72 55.57	67.16	15.83		*74.41* (74.06)	*81.78* (81.18)	*30.67* (30.82)
P2		50.43 46.77	57.78	8.06		*59.94* (60.19)	*67.19* (67.21)	*17.88* (18.47)
P3		44.39	51.26	2.96		*56.55* (57.61)	*63.01* (64.15)	*15.77* (16.86)
P4		74.85 68.51	87.75	− 6.53		*101.95* (100.92)	*114.71* (113.76)	*20.89* (19.78)
P5		123.61 118.30	137.56	40.96		*142.1* (142.57)	*156* (156.7)	*59.58* (59.35)

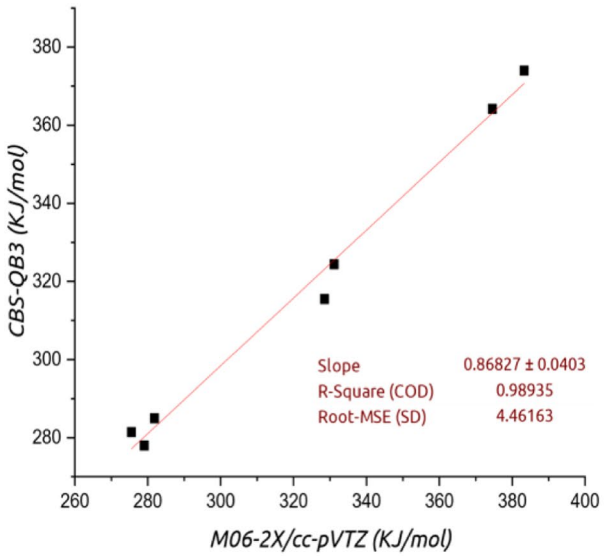

a) The correlation of barrier heights between CBS-QB3 method and M06-2X/cc-pvTZ level.

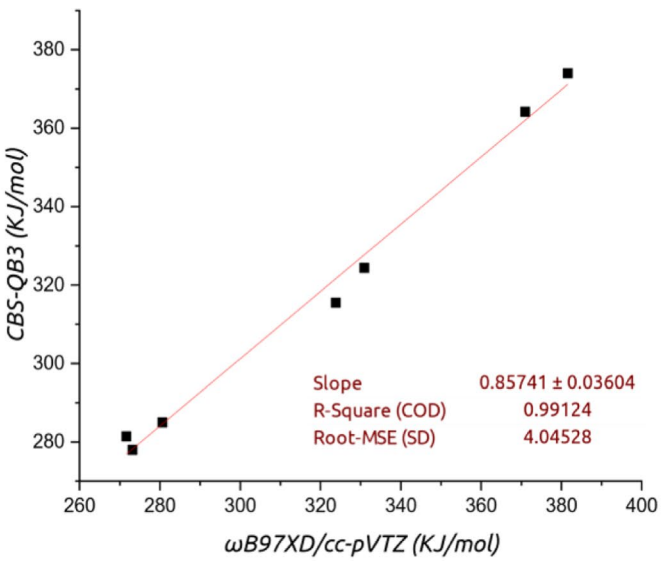

b) The correction of barrier heights between CBS-QB3 method and ωB97XD /cc-pvTZ level.

Fig. 7 Correlation between barrier heights (kJ/mol) at the CBS-QB3 method aganist that obtained at M06-2X/cc-pvTZ level (Fig. 7a) and at ωB97XD /cc-pvTZ level (Fig. 7b)

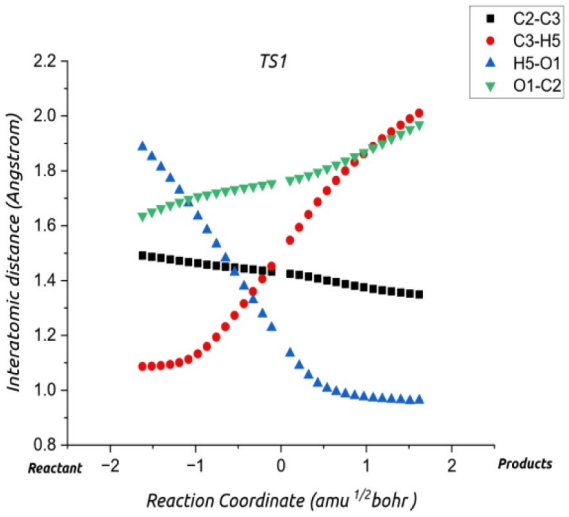

a) Changes of bond length along with IRC during TS1

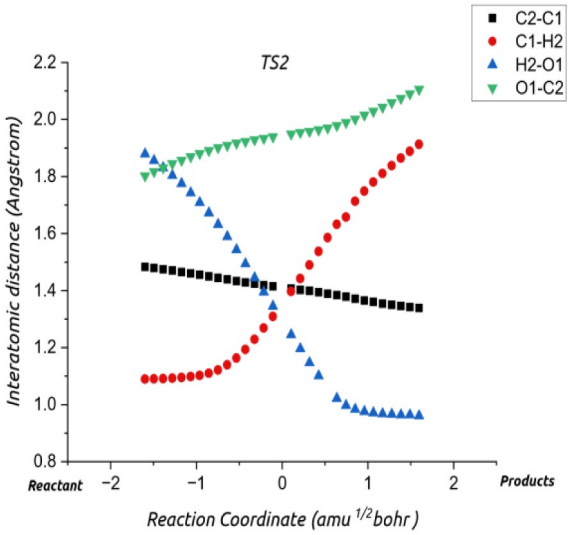

b) Changes of bond length along with IRC during TS2

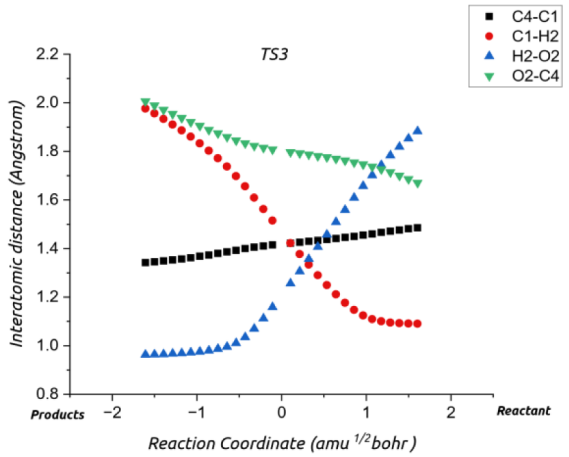

c) Changes of bond length along with IRC during TS3

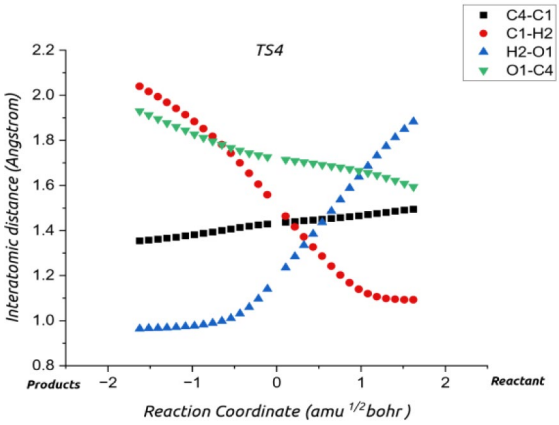

d) Changes of bond length along with IRC during TS4

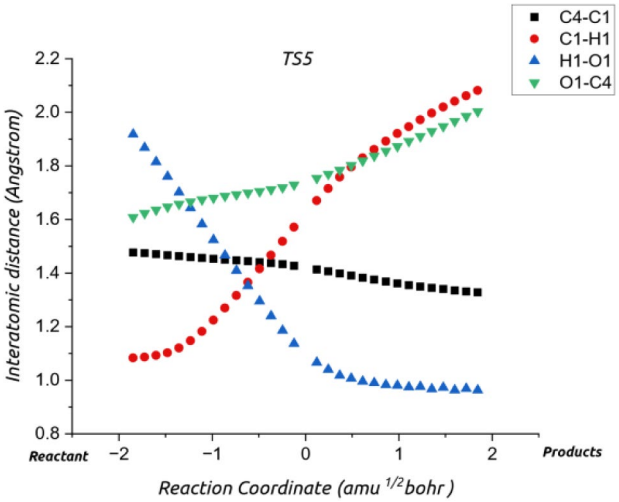

e) Changes of bond length along with IRC during TS5

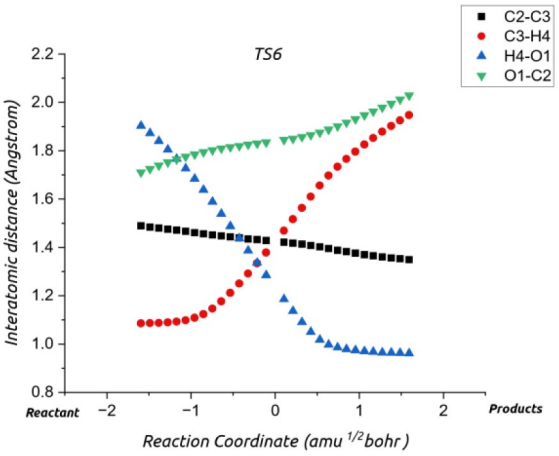

f) Changes of bond length along with IRC during TS6

Fig. 8 Changes of bond length along with IRC for all 1, 3-BDO dehydration reactions at M06-2X/cc-pVTZ level of theory

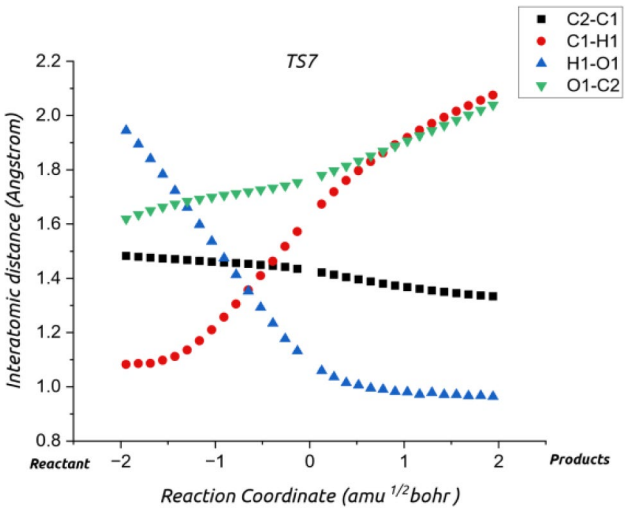

g) Changes of bond length along with IRC during TS7

Fig. 8 (continued)

meta-functional incorporates 54% Hartree–Fock (HF) exchange [33], compared to only 20% HF exchange for B3LYP functional used in CBS-QB3 method [35]. The IRC calculations revealed that the transition state effectively connect the reactant to their corresponding products.

Detailed bonds lengths variations versus IRC for complex fission reactions are presented in Fig. 8, while Figures S2-S8 (In the supporting file (SI)) display the potential energy profiles along MEP of 1, 3-BDO dehydration at M06-2X/cc-pvTZ level.

The IRCs for the formation of 1-buten-4-ol is shown in Fig. 8a. The figure illustrates the rapid rapture of the strong O1-C2 bond (BDE = 415.2 kJ/mol). The broken C3-H5 bond at s = − 0.3 amu$^{1/2}$ bohr is associated with the formation of the H5-O1 bond, where the two curves intersect at the transition state (s = − 0.2 amu$^{1/2}$bohr). The formation of the C2-C3 double bond occurs gradually during the reaction.

Figure 8b indicates a more pronounced rupture of the O1-C2 bond to the C1-H1 bond. The dissociation of the C1-H2 bond begins at s = 0.0 amu$^{1/2}$ bohr, while the formation of the H2-O1 bond progresses simultaneously with breaking of the C1-H2 bond. The two curves cross each other at s = 0.0 amu$^{1/2}$bohr.

Figure 8c illustrates a rapid cleavage of the O2-C4 bond (408.8 kJ/mol) relative to the weaker C1-H2 bond (BDE = 324.3 kJ/mol), which occurs at s = 0.8 amu$^{1/2}$bohr. The formation of the H2-O2 bond begins at s = − 0.4 amu1/2bohr. The two curves of C1-H2 and H2-O2 bonds cross each other at s = 0.3 amu1/2bohr, while the formation of the double π bond betweenC4 and C1 occurs gradually during the reaction.

The changes on bond length along the IRC for the formation of P4 is shown in Fig. 8d. The Figure demonstrates that the weakest C1-H2 bond (BDE = 324.3 kJ/mol) dissociates earlier (at s = 0.8 amu$^{1/2}$bohr) than the strong alcoholic O1-C4 bond (BDE = 408.8 kcal/mol), which raptures at s = 0.3 amu$^{1/2}$bohr.

The H2-O1 bond is formed at s = − 0.2 amu$^{1/2}$bohr, while the double C4-C1 bond is formed smoothly during the reaction. The curves for the C1-H2 and H2-O1 bonds cross each other at s = 0.3 amu$^{1/2}$bohr. Figure 8e illustrates the variation of selected bonds lengths during TS5. The breaking of the C1-H1 bond occurs first at s = − 1.1 amu$^{1/2}$bohr, followed by rapture of the O1-C4 bond s = 0.1 amu$^{1/2}$bohr, while the formation of the C4-C1 double bond progresses smoothly during the reaction. According to Fig. 8f, the O1-C2 bond is broken first (at s = − 0.5 amu$^{1/2}$bohr), followed by the slow stretching of the C3-H4 bond until it raptures at s = − 0.3 amu$^{1/2}$bohr. The breaking of the C3-H4 bond and the formation of the H4–O1 bond occur simultaneously, with the two curves intersecting at s = − 0.1 amu$^{1/2}$bohr. The investigation of IRC in Fig. 8g indicates a rapid breakage of the O1–C2 bond at s = 0.0 amu$^{1/2}$bohr, while the C1–H1 bond stretches and breaks at s = − 0.5 amu$^{1/2}$bohr, accompanied by the formation of the H1–O2 bond. The two curves intersect at s = 0.7 amu$^{1/2}$bohr.

4 Conclusion

In this study, we explore the thermochemical aspects of the dehydration mechanism of the bifunctional biofuel 1, 3-butanediol (1, 3-BDO) by constructing the potential energy profile for different dehydration reactions using various computational chemistry methods. The computational study has been performed using the DFT/ M06-2X and ωB97XD methods in conjunction with the correlation consistent polarized valence triplet zeta (cc-pvTZ) and the ab initio complete basis set – quadratic Becke3 (CBS-QB3).

Investigation of bond dissociation energies (BDEs) reveals that terminal C2–C3 bond has the lowest value (BDEs = 361 kJ/mol) among all C–C and C–O bonds, indicating that it will be particularly susceptible during the combustion of 1, 3-BDO at high temperature. The BDEs of the terminal alcoholic OH group (BDEs = 409 kJ/mol) is lower compared to that of internal OH group (BDEs = 415 kJ/mol). These results align with previous literatures for n-butanol, 2-butanol, and 2-Methoxyethanol. From BDEs results, the results suggest that the rapid disintegration of the terminal OH group indicates that the initiation of the dehydration

reaction will occur through the removal the terminal OH group.

The finding is consistent with the potential energy profile, which indicates that the formation of the final product 1, 3-butadiene (1,3-BD, P4), occurs via transition states TS4 and TS6. The formation of 1,2-butadiene (1,2-BD, P5) is less likely due to the instability of the allene structure.

Supplementary Information The online version contains supplementary material available at https://doi.org/10.1007/s00214-024-03154-5.

Acknowledgements This work was supported by the Fund of Ministry of Education (No. 8091B032244), the Open Fund of the State Key Laboratory of Engines of China (No. K2023-11), the Open Fund of the Ministry Key Laboratory of Marine Power Engineering and Transport Technology (No. KLMPET2022-01), and the Space Power Fund of the China Space Foundation (No. KDJJ20230202005).

Author contributions Mohamed A. Abdel-Rahman: Conceptualization, Data curation, Formal analysis, Investigation, Writing – review & edit. Response to Reviewer's comments. Mohammed K. Morse: Conceptualization, Data curation, Formal analysis, Investigation, Writing – review & edit. Hao Zhao: Supervision, Writing – review & edit.

Data availability All data analyzed in the study are available upon request. No datasets were generated or analysed during the current study.

Declarations

Conflict of interest The authors declare that they have no known competing financial interests or personal relationships that could have appeared to influence the work reported in this paper.

References

1. Hanaki K, Portugal-Pereira J (2018) The effect of biofuel production on greenhouse gas emission reductions. In: Takeuchi K, Shiroyama H, Saito O, Matsuura M (eds) Biofuels and sustainability: holistic perspectives for policy-making. Springer, Tokyo, pp 53–71. https://doi.org/10.1007/978-4-431-54895-9_6
2. El-Nahas AM, Mangoo AH, El-Meleigy AB (2012) A computational study on the structures and energetics of isobutanol pyrolysis. Comput Theor Chem 997:94–102. https://doi.org/10.1016/j.comptc.2012.08.009
3. Balamurugan T, Nalini R (2014) Experimental investigation on performance, combustion and emission characteristics of four stroke diesel engine using diesel blended with alcohol as fuel. Energy 78:356–363
4. Agarwal AK (2007) Biofuels (alcohols and biodiesel) applications as fuels for internal combustion engines. Prog Energy Combust Sci 33(3):233–271. https://doi.org/10.1016/j.energy.2014.10.020
5. Al-Otaibi JS, Abdel-Rahman MA, Almuqrin AH, El-Gogary TM, Mahmoud MA, El-Nahas AM (2021) Thermo-kinetic theoretical studies on pyrolysis of dimethoxymethane fuel additive. Fuel 290:119970
6. Abdel-Rahman MA, Al-Hashimi N, Shibl MF, Yoshizawa K, El-Nahas AM (2019) Thermochemistry and kinetics of the thermal degradation of 2-methoxyethanol as possible biofuel additives. Sci Rep 9(1):4535
7. Abdel-Rahman MA, El-Gogary TM, Al-Hashimi N, Shibl MF, Yoshizawa K, El-Nahas AM (2019) Computational studies on the thermodynamic and kinetic parameters of oxidation of 2-methoxyethanol biofuel via H-atom abstraction by methyl radical. Sci Rep 9(1):15361
8. Abdel-Rahman MA, Shiroudi A, Czub J, Zhao H (2024) Screening stability, thermochemistry, and chemical kinetics of 3-hydroxybutanoic acid as a bifunctional biodiesel additive. J Phys Chem A 128:4068–4082
9. Gräfje H, Körnig W, Weitz HM, Reiß, W., Steffan, G., Diehl, H., Kieczka, H. (2000). Butanediols, butenediol, and butynediol. Ullmann's Encycl Ind Chem. https://doi.org/10.1002/14356007.a04_455
10. National Center for Biotechnology Information (2023). PubChem Compound Summary for CID 7896, 1,3-Butanediol
11. Matsuyama A, Yamamoto H, Kawada N, Kobayashi Y (2001) Industrial production of (R)-1,3-butanediol by new biocatalysts. J Mol Catal B Enzym 11:513–521
12. Kataoka N, Vangnai AS, Tajima T, Nakashimada Y, Kato J (2013) Improvement of (R)-1,3-butanediol production by engineered Escherichia coli. J Biosci Bioeng 115(5):475–480
13. Liu L, Asano T, Nakagawa Y, Tamura M, Tomishige K (2020) One-pot synthesis of 1,3-butanediol by 1,4-anhydroerythritol hydrogenolysis over a tungsten-modified platinum on silica catalyst. Green Chem 22(8):2375–2380
14. Moss JT, Berkowitz AM, Oehlschlaeger MA, Biet J, Warth V, Glaude P-A, Battin-Leclerc F (2008) An experimental and kinetic modeling study of the oxidation of the four isomers of butanol. J Phys Chem A 112:10843–10855. https://doi.org/10.1021/jp806464p
15. Pelucchi M, Namysl S, Ranzi E, Rodriguez A, Rizzo C, Somers KP, Faravelli T (2020) Combustion of n-C3–C6 linear alcohols: an experimental and kinetic modeling study. Part II: Speciation measurements in a jet-stirred reactor, ignition delay time measurements in a rapid compression machine, model validation, and kinetic analysis. Energy & Fuels 34(11):14708–14725. https://doi.org/10.1021/acs.energyfuels.0c02252
16. Liu B, Zhu Q, Zhu L, Xie C, Xu Q, Wang Z (2024) Low-temperature oxidation of n-butanol in a jet-stirred reactor: Detailed species measurements and modeling studies. Combust Flame 261:113290
17. El-Nahas AM, Mangood AH, Takeuchi H, Taketsugu T (2011) Thermal decomposition of 2-butanol as a potential nonfossil fuel: a computational study. J Phys Chem A 115:2837–2846
18. Sarathy SM, Thomson MJ, Togbé C, Dagaut P, Halter F, Mounaim-Rousselle C (2009) An experimental and kinetic modeling study of n-butanol combustion. Combust Flame 156(4):852–864
19. Harper MR, Van Geem KM, Pyl SP, Marin GB, Green WH (2011) Comprehensive reaction mechanism for n-butanol pyrolysis and combustion. Combust Flame 158(1):16–41
20. Cai J, Zhang L, Zhang F, Wang Z, Cheng Z, Yuan W, Qi F (2012) Experimental and kinetic modeling study of n-butanol pyrolysis and combustion. Energy Fuels 26(9):5550–5568
21. Cai J, Yuan W, Ye L, Cheng Z, Wang Y, Zhang L, Zhang F, Li Y, Qi F (2013) Experimental and kinetic modeling study of 2-butanol pyrolysis and combustion. Combust Flame 160(10):1939–1957
22. Liu H, Li S, Zheng Z, Xu J, Yao M (2013) Effects of n-butanol, 2-butanol, and methyl octynoate addition to diesel fuel on combustion and emissions over a wide range of exhaust gas recirculation (EGR) rates. Appl Energy 112:246–256
23. Zheng J, Oyedepo GA, Truhlar DG (2015) Kinetics of the hydrogen abstraction reaction from 2-butanol by OH radical. J Phys Chem A 119(50):12182–12192
24. Black G, Simmie JM (2010) Barrier heights for H-atom abstraction by HȮ2 from n-butanol—A simple yet exacting test for model chemistries? J Comput Chem 31(6):1236–1248

25. Thion S, Zaras AM, Szőri M, Dagaut P (2015) Theoretical kinetic study for methyl levulinate: oxidation by OH and CH3 radicals and further unimolecular decomposition pathways. Phys Chem Chem Phys 17:23384–23391
26. Jin ZH, Xu DH, Hang CZ, Pan GF, Zhang HY, Tian ZY (2024) Experimental and kinetic study on 2-methoxyethanol part I: Molecular chemistry and pyrolysis investigation. Combust Flame 260:113238
27. Abdel-Rahman MA, El-Demerdash SH, El-Nahas AM (2017) Theoretical studies on thermochemistry and kinetics of hydrogen abstraction from 2-methoxyethanol by hydrogen atom. Int J Adv Sci Technol Res 2:203–213
28. Ward DJ, Saccomando DJ, Walker G, Mansell SM (2023) Sustainable routes to alkenes: applications of homogeneous catalysis to the dehydration of alcohols to alkenes. Catal Sci Technol 13(9):2638–2647. https://doi.org/10.1039/D2CY01690G
29. Sun D, Arai S, Duan H, Yamada Y, Sato S (2016) Vapor-phase dehydration of C4 unsaturated alcohols to 1,3-butadiene. Appl Catal A: Gen. https://doi.org/10.1016/j.apcata.2016.11.035
30. Kurniawan E, Yu L, Kobayashi R, Hara T, Yamada Y, Sato S (2023) Vapor-phase dehydration of 1,3-butanediol to 1,3-butadiene over WO3/SiO2 catalyst. Appl Catal A Gen. https://doi.org/10.1016/j.apcata.2023.119408
31. Frisch MJ, Trucks GW, Schlegel HB, Scuseria GE, Robb MA, Cheeseman JR, et al. Gaussian, Inc. Wallingford CT: Gaussian 09.
32. Frisch MJ, Trucks GW, Schlegel HB, Scuseria GE, Robb MA, Cheeseman JR, et al. Gaussian, Inc. Wallingford CT: Gaussian 16.
33. Zhurko GA (2014) Chemcraft Program V.1.6. https://www.chemcraftprog.com.
34. Zhao Y, Truhlar DG (2008) The M06 suite of density functionals for main group thermochemistry, thermochemical kinetics, noncovalent interactions, excited states, and transition elements: two new functionals and systematic testing of four M06-class functionals and 12 other functionals. Theoret Chem Acc 120(3–6):215
35. Chai JD, Head-Gordon M (2008) Long-range corrected hybrid density functionals with damped atom-atom dispersion corrections. Phys Chem Chem Phys 10:6615–6620. https://doi.org/10.1039/B810189B
36. Montgomery JA Jr, Frisch MJ, Ochterski JW, Petersson GA (1999) A complete basis set model chemistry. VII. Use of density functional geometries and frequencies. J Chem Phys 11:2822–2827
37. Montgomery JA Jr, Frisch MJ, Ochterski JW, Petersson GA (2000) A complete basis set model chemistry. VII. Use of the minimum population localization method. J Chem Phys 11:6532–6542
38. Pokon EK, Liptak MD, Feldgus S, Shields GC (2001) Comparison of CBS-QB3, CBS-APNO, and G3 predictions of gas phase deprotonation data. J Phys Chem A 105:10483–10487
39. Ochterski JW, Petersson GA, Montgomery JA (1996) A complete basis set model chemistry 0.5. Extensions to six or more heavy atoms. J Chem Phys. 104:2598–2619
40. Gonzalez C, Schlegel HB (1989) An improved algorithm for reaction path following. J Chem Phys 90:2154–2161
41. Gonzalez C, Schlegel HB (1990) Reaction path following in mass-weighted internal coordinates. J Phys Chem 94:5523–5527
42. Rayne S, Forest K (2011) Estimated adiabatic ionization energies for organic compounds using the Gaussian-4 (G4) and W1BD theoretical methods. J Chem Eng Data 56:350–355. https://doi.org/10.1021/je100913f
43. Lewars EG (2011) Computational chemistry, introduction to the theory and applications of molecular and quantum mechanics, 3rd edn. Springer, New York
44. Carles S, Desfrancois C, Schermann JP, Jalbout AF, Adamowicz L (2001) Dipole-bound anion of 1,3-butanediol: Ab initio and Rydberg electron transfer spectroscopy study. Chem Phys 334:374–380. https://doi.org/10.1016/S0009-2614(00)01455-X
45. Holmes JL, Lossing FP (1983) The need for adequate thermochemical data for the interpretation of fragmentation mechanisms and ion structure assignments. Int J Mass Spectrom Ion Phys 47:133. https://doi.org/10.1016/0020-7381(83)87154-X
46. Traeger JC, McAdoo DJ (1986) Decomposition thresholds and associated translational energy releases for eight $C_4H_8O^+$ isomers. Int J Mass Spectrom Ion Process 68:35. https://doi.org/10.1016/0168-1176(86)87066-5
47. Mallard WG, Miller JH, Smyth KC (1983) The ns Rydberg series of 1,3-trans-butadiene observed using multiphoton ionization. J Chem Phys 79:5900. https://doi.org/10.1063/1.445770
48. Bieri G, Burger F, Heilbronner E, Maier JP (1973) Valence ionization energies of hydrocarbons. Helv Chim Acta 60:2213. https://doi.org/10.1002/hlca.19770600714
49. Snow KB, Thomas TF (1990) Mass spectrum, ionization potential, and appearance potentials for fragment ions of sulfuric acid vapor. Int J Mass Spectrum Ion Process 96:49. https://doi.org/10.1016/0168-1176(90)80041-Z
50. Peel JB, Willett GD (1975) Photoelectron spectroscopic studies of the higher alcohols. Aust J Chem 28:2357. https://doi.org/10.1071/CH9752357
51. Shao JD, Baer T, Lewis DK (1988) Dissociation dynamics of energy-selected ion-dipole complexes. 2. Butyl alcohol ions. J Phys Chem 92:5123–5128. https://doi.org/10.1021/j100329a014
52. Holmes JL, Lossing FP (1991) Ionization energies of homologous organic compounds and correlation with molecular size. Org Mass Spectrom 26:537. https://doi.org/10.1002/oms.1210260603
53. Luo Y-R, Pacey PD (1992) Effects of alkyl substitution on ionization energies of alkanes and haloalkanes and on heats of formation of their molecular cations. Part 2. Alkanes and chloro-, bromo- and iodoalkanes. Int J Mass Spectrom Ion Process 112:63. https://doi.org/10.1016/0168-1176(92)87032-A
54. Cocksey BJ, Eland JHD, Danby CJ (1971) The effect of alkyl substitution on ionisation potential. J Chem Soc. https://doi.org/10.1039/J29710000790
55. Berkowitz J, Greene JP, Cho H, Ruscic B (1987) The ionization potentials of CH_4 and CD_4. J Chem Phys 86:674. https://doi.org/10.1063/1.452268
56. Bowen RD, Maccoll A (1984) Low energy, low temperature mass spectra. Org Mass Spectrom 19:379. https://doi.org/10.1002/oms.1210190806
57. Bissonnette M, George M, Holmes JL (1990) The experimental investigation of $[C_5H_{12}O]$ ion structures related to neopentyl alcohol and its methyl ether. Int J Mass Spectrom Ion Processes 101:309. https://doi.org/10.1016/0168-1176(90)87019-D
58. Ashmore FS, Burgess AR (1977) Study of some medium size alcohols and hydroperoxides by photoelectron spectroscopy. J Chem Soc Faraday Trans 2(73):1247. https://doi.org/10.1039/F29777301247
59. Stockbauer R, Inghram MG (1971) Experimental relative Franck–Condon factors for the ionization of methane, ethane, and propane. J Chem Phys 54:2242. https://doi.org/10.1063/1.1675158
60. Moureu and Dode (1937) Chaleurs de formation de l'oxyde d'ethylene, de l'ethanediol et de quelques homologues. Bull Soc Chim France 1937(4):637–647
61. Prosen EJ, Maron FW, Rossini FD (1951) Heats of combustion, formation, and insomerization of ten C_4 hydrocarbons. J Res NBS 46:106–112. https://doi.org/10.6028/jres.046.015
62. Prosen EJ, Maron FW, Rossini FD (1949) Heat of isomerization of the two butadienes. J Res NBS 42:269–275
63. Chase MW Jr (1998) NIST-JANAF Thermochemical Tables, Fourth Edition. J. Phys. Chem. Ref. Data Monograph 9:1–1951.
64. Manion JA (2002) Evaluated enthalpies of formation of the stable closed shell C1 and C2 chlorinated hydrocarbons. J Phys Chem Ref Data 31(1):123–172. https://doi.org/10.1063/1.1420703

65. Afeefy HY, Liebman JF, Stein SE Gas Phase Thermochemical Data. In: Linstrom PJ, Mallard WG, Eds. NIST Chemistry WebBook, NIST Standard Reference Database Number 69; National Institute of Standards and Technology: Gaithersburg, MD; http://webbook.nist.gov (2023).
66. Pittam DA, Pilcher G (1972) Measurements of heats of combustion by flame calorimetry. Part 8.-Methane, ethane, propane, n-butane and 2-methylpropane. J Chem Soc Faraday Trans 1(68):2224–2229. https://doi.org/10.1039/F19726802224
67. Ruscic B, Pinzon RE, Morton ML, von Laszewski G, Bittner S, Nijsure SG, Amin KA, Minkoff M, Wagner AF (2004) Introduction to active thermochemical tables: several "key" enthalpies of formation revisited. J Phys Chem A 108:9979–9997. https://doi.org/10.1021/jp047912y
68. Ruscic B, Pinzon RE, von Laszewski G, Kodeboyina D, Burcat A, Leahy D, Montoya D, Wagner AF (2005) Active thermochemical tables: thermochemistry for the 21st century. J Phys Conf Ser 16:561–570. https://doi.org/10.1088/1742-6596/16/1/078
69. Ruscic B, Bross DH (2024) Active Thermochemical Tables (ATcT) values based on ver. 1.202 of the Thermochemical Network available at ATcT.anl.gov.
70. Ruscic B, Bross DH (2024) Accurate and Reliable thermochemistry by data analysis of complex thermochemical networks using active thermochemical tables: the case of glycine thermochemistry. Faraday Discuss. https://doi.org/10.1039/D4FD00110A
71. Ruscic B (2014) Uncertainty quantification in thermochemistry, benchmarking electronic structure computations, and active thermochemical tables. Int J Quantum Chem 114:1097–1101. https://doi.org/10.1002/qua.24605
72. Ruscic B, Bross DH (2019) Thermochemistry. Computer aided. Chem Eng 45:3–114. https://doi.org/10.1016/B978-0-444-64087-1.00001-2
73. Hammond GS (1955) A correlation of reaction rates. J Am Chem Soc 77:334–338. https://doi.org/10.1021/ja01607a027